IEEE Robotics and Automation Letters (RAL) paper presented at the
2020 IEEE International Conference on Robotics and Automation (ICRA)
31 May - 31 August, 2020. Paris, France

VaLeNS: Design of a novel Variable Length Nested Soft Arm

Naveen Kumar Uppalapati[1] and Girish Krishnan[1]

***Abstract*— Over the last decade, soft continuum arms (SCAs) have successfully demonstrated the compliance and dexterity needed to operate in unstructured environments and handle fragile objects. However, their inherent soft compliance limits their performance in situations where stiffness and force transfer is required. In this letter, we present a compact design architecture, which is a hybrid between soft arms and rigid links known as Variable Length Nested Soft (VaLeNS) arm. The design architecture involves a novel SCA nested inside a concentric rigid tube. The SCA can undergo a combination of spatial bending (B) and bidirectional axial twist (R^2), and can extrude out or retract back into the rigid tube with varying length. The resulting configuration is shown to modulate stiffness up to a factor of ten and exhibits enhanced workspace and dexterity. Furthermore, the VaLeNS arm mounted on a rigid robotic platform allows for bifurcation of the overall workspace into rigid and soft, and can achieve high reachability in constrained environments. The paper demonstrates the effectiveness of the VaLeNS arm system in manipulation tasks that require both the rigid and soft attributes. This design architecture is deemed useful in agricultural applications and in physical human robot interaction.**

I. Introduction

Soft Continuum Arms (SCAs) or manipulators are useful especially in applications that demand dexterity, safety under human interactions, and adaptability [1]. These robots are composed of materials with extremely low elastic moduli [2] that undergo material deformation actuated either by cables [3], [4], [5] or fluids [6], [7], [8]. Their usefulness has been demonstrated in whole arm grasping and manipulation [9] in unstructured environments such as rescue operations, assisting in activities of daily living [10], and as an additional wearable limb [11].

There are a number of limitations with SCAs that prompt additional considerations: **(i)** While adaptable, their soft and squishy nature may not lend itself to precise operations that require transmitting large loads to the object. These are usually attributes of rigid robots. The closest to fulfilling these requirements are variable stiffness robots [12], [13]. **(ii)** Most SCAs use bending as a mode of deformation and thus require two or more serial segments that are independently controlled to achieve sufficient workspace and dexterity. The serial construction increases complexity and weight, and requires additional valves and hoses running through the body [14], [15]. **(iii)** Though dexterous, most SCAs have limited reach or steerability for navigation in constrained environments. Continuum robots that have shown promise are the concentric tube robots [16] and pneumatically folded inflating chambers that grow [17].

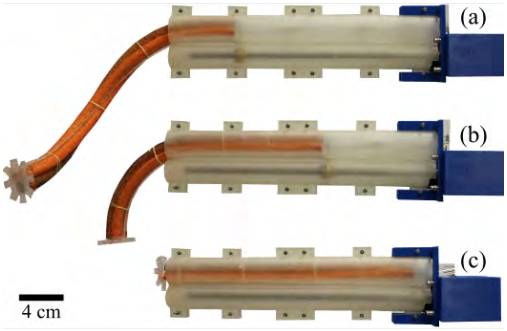

Fig. 1. The **Va**riable **Le**ngth **N**ested **S**oft arm or VaLeNS arm with (a) the soft arm completely extruded, (b) partially extruded, and (c) completely retracted within a rigid shell.

In this paper, we present a new design concept (in Sec.II), which is a hybrid between soft and rigid arms to overcome these limitations. The **Va**riable **Le**ngth **N**ested **S**oft arm or VaLeNS arm consists of a single segment SCA nested inside a concentric rigid shell (Fig. 1). Inspired by the concentric tube continuum robots [16], an internal mechanism is used to extrude out or retract the SCA back into the shell. When the entire arm is extended out of the shell, the robot is considered soft (Fig. 1(a)), while when enclosed completely within the shell, it is considered rigid (Fig. 1(c)). The SCA used has a unique asymmetric architecture that can simultaneously Bend (B) and Rotate in clockwise and counterclockwise (R^2) directions leading to spatial deformation.

We hypothesize that the VaLeNS arm with a BR^2 SCA exhibits two fundamental attributes namely **(i)** an enhanced workspace and dexterity, and **(ii)** the ability to modulate stiffness and transfer impact forces. This paper studies these attributes in detail using a combination of computational models and experiments (in Sec. III and Sec. IV). Furthermore, these fundamental attributes lead to several derived functionalities that make the architecture useful. Two most important are **(a)** hybrid workspace and **(b)** enhanced reachability or steerability.

Hybrid workspace refers to the part of the workspace where the SCA behaves as a rigid robot (such as in Fig. 1(c)) capable of quick, precise operations that include transmission of loads. We demonstrate this feature with a door opening task (in Sec. V) where sufficient forces are needed to be transmitted to the knob for successful operation. The other part of the workspace where the arm is sufficiently extruded can be used for adaptable and safe manipulation with suffi-

The work is jointly funded by NIFA through the NIFA-NSF National Robotics Initiative (USDA 2019-67021-28989)

[1]These authors are with the department of Industrial and Enterprise Systems Engineering at the University of Illinois Urbana-Champaign (UIUC), Urbana, IL 61801 USA {uppalap2, gkrishna}@illinois.edu

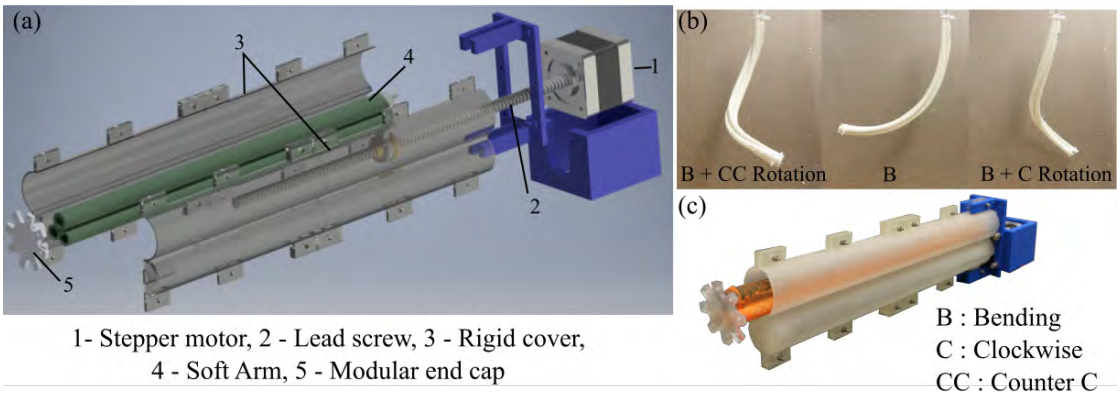

Fig. 2. VaLeNS arm: (a) Different components and their assembly. (b) The different deformation modes of BR^2 SCA (B:Bending, C: Clockwise rotation and CC: Counterclockwise rotation). (c) Fabricated prototype of the VaLeNS arm used in this work.

cient dexterity. We demonstrate this feature on a task where the robot end effector fixed with a sharp scalpel interacts safely with a skin like membrane. The second feature is reachability, which is a function of extrusion out of the rigid shell and the simultaneous curvilinear deformation of the SCA. We demonstrate that a VaLeNS arm is able to reach an object by avoiding at least two closely-spaced obstacles (in Sec. V).

The VaLeNS arm can be used in several applications that require the hybrid workspace and reachability features. For example, in automated berry harvesting, reachability is important in approaching, imaging and picking berries that are occluded inside bushes, thus necessitating the soft arm, while those on the periphery can be picked rather quickly using the rigid arm alone. Furthermore, the hybrid workspace feature is important in collaborative robot-human applications especially in manufacturing, where a combination of precise operations and safe interactions are required.

II. Design and Fabrication of VaLeNS Arm

Our prototype hybrid arm, shown in Fig. 2(c) consists of a Soft Continuum Arm (SCA), a rigid enclosure and a hybrid actuation system. The rigid enclosure houses the SCA and a mechanism to extrude or retract the arm. We provide a detailed description of each module in following subsections.

A. Rigid Enclosure

The rigid enclosure consists of a NEMA 17-size hybrid bipolar stepper motor (marked 1 in Fig. 2a) that has an integrated 28 cm threaded rod (marked 2 in Fig. 2a) as its output shaft (Pololu). This arrangement converts the motor into a linear actuator capable of precision open loop positioning. The travel nut is attached to the base of the SCA. A two part cylindrical rigid enclosure (marked 3 in Fig. 2a) that houses the SCA is 3D printed. The rigid enclosure restricts the rotational degree of freedom of the SCA when attached to the travel nut. In addition, the rigid enclosure also restricts the deformation (bending or axial rotation) of the portion of the SCA enclosed. 3D printed parts are used to attach the rigid enclosure to the stepper motor.

B. SCA design

The BR^2 Soft Continuum Arm (SCA) consists of a parallel combination of three pneumatically actuated Fiber Reinforced Elastomeric Enclosures (FREEs) [7], [18] that can bend, and rotate in clockwise and counterclockwise directions respectively. A combination of spatial bending and axial twist or rotation results in a spiral deformation mode [19], which yields a large spatial workspace and dexterity (its deformation modes shown in Fig. 2(b)) with a compact design. Furthermore, the BR^2 design can achieve variable stiffness in its pure bending configuration by differential pressurization of the bending and rotating FREEs. In Section III, we demonstrate that the workspace, dexterity and stiffness modulating ability can be enhanced in the varying length hybrid arrangement.

Apart from pneumatic actuation, other actuation schemes such as tendon driven and shape memory alloys can be considered. However, we choose pneumatic actuation for its compactness, moderate to high bandwidth and ease in controls and implementation.

The SCA has a modular end cap at the distal end, which can be mounted with an end effector such as a camera or a gripper. The SCA is attached to the rigid enclosure with a custom 3D printed part and can extrude out of or retract back into the rigid enclosure.

C. Hybrid actuation

The VaLeNS system is actuated by a combination of stepper motors and pressurized air. The actuation signals for the stepper motor (controlled by a Big Easy Driver) and pressure channels in the SCA are generated using a National Instruments myRIO embedded device. SMC valves (ITV0031-2UBL) are used to regulate the pressure in the SCA.

The stepper motor of VaLeNS arm is attached to a rotating servo which provides axial rotation to the VaLeNS arm in order to achieve more workspace. The entire VaLeNS arm weighs 550 gms and can be retrofitted to any commercial robot platform.

III. Analytical and Experimental Methods

The VaLeNS arm exhibits two important primary attributes: (a) Enhanced workspace and dexterity, and (b) ability to modulate stiffness and impact forces. To conduct studies on these attributes we utilize a combination of modeling and experiments, which are detailed in this section. Furthermore, when the VaLeNS arm is deployed in an existing robotic platform, it exhibits two important derived features, namely hybrid workspace and reachability. Specifically, this section also details the deployment of the VaLeNS arm on a commercial RRR robot.

A. Forward Kirchhoff Model for the BR^2 SCA

The Kirchhoff model is an analytical model that predicts the deformed shape of a continuum robot [20] under the action of external loads. The same method is also shown to approximately predict the shape of pneumatically actuated SCAs [21], [19], [7]. The Kirchhoff model was previously presented for the BR^2 SCA in [22] to predict the final deformed curve for different actuation pressures and a condensed overview is presented here. The following Kirchhoff rod equations are used to obtain the end shape of the manipulator.

$$\dot{\mathbf{p}} = \mathbf{Re} \tag{1}$$

$$\dot{\mathbf{R}} = \mathbf{R}\hat{\mathbf{u}} \tag{2}$$

$$\dot{\mathbf{u}} = -\mathbf{C^{-1}}(\hat{\mathbf{u}}\mathbf{C}(\mathbf{u}-\mathbf{u_0}) + \hat{\mathbf{e}}\mathbf{R^T}(\mathbf{f_b}(\mathbf{L}-\mathbf{s})\mathbf{ge_g} + \mathbf{f_e})) \tag{3}$$

$\mathbf{p} \in \mathbb{R}^3$ is the position vector, $\mathbf{R} \in SO(3)$ is the rotation matrix, $\mathbf{u} \in \mathbb{R}^3$ is the material curvatures and twist for $s \in [0, L]$. L is the total length of the actuator, $\mathbf{f_b}$ is mass per unit length of the SCA, $\mathbf{f_e}$ is the end weight on the soft arm. $\hat{a}$ is the skew symmetric matrix for any vector a, $\mathbf{g}$ is acceleration due to gravity and $\mathbf{u_0}$ is the pre-curvature vector of the SCA. $\mathbf{e_g}$ is the direction of gravity and $\mathbf{C}$ is collection of bending and twisting stiffness matrix. The actuation of the BR^2 SCA is through the pre-curvatures $\mathbf{u}_0$, which can be represented as a function of applied pressure. In an ideal scenario, pressurizing the bending FREEs lead to a constant curvature bending while pressurizing the rotating FREEs lead to uniform torsion (twist per unit length). When both bending and rotating FREEs are triggered simultaneously, an attenuation is reported due to coupling [7], where the bending curvature is reduced due to the stiffness of the rotating FREEs and vice versa. Our previous effort quantifies the coupling [7] and presents a method to estimate the Kirchhoff rod parameters such as the pre-curvatures $\mathbf{u_0}$ and flexural modulii $\mathbf{C}$ using a parameter estimation method. The readers are requested to refer to authors previous work [7], [22] for detail steps in obtaining the actuation ($\mathbf{u_0}$) and stiffness ($\mathbf{C}$) parameters.

With these as input, the set of differential equations given in Eqs. 1-3 can be solved to estimate the overall shape of the manipulator. In this paper, the "bvp4c" routine in MATLAB is used to solve this forward model. The initial $\mathbf{p}$ and $\mathbf{R}$ are the end position and orientation of the rigid enclosure. Furthermore, the boundary condition at the manipulator end $s = L$ is given as $\mathbf{u} = \mathbf{u_0}$. Using these boundary conditions and the estimated parameters the final shape is obtained.

B. Evaluating Workspace and Dexterity

Workspace involves the collection of end effector positions that the VaLeNS arm can reach for its operating range of input pressures. We evaluate the workspace of the VaLeNS arm mounted on a swivel base oriented along the z (or gravity) axis. The swiveling base is used to rotate the end point to lie in $y-z$ plane. The resulting workspace will be a surface (in the $y-z$ plane) that can be axisymmetrically rotated about the arm axis(z axis). The forward model is used to evaluate the axisymmetric workspace by simulating the bending pressure P_b, rotating pressures (clockwise P_{rc} and counterclockwise P_{rcc}) and lengths L in the ranges of 75.8423 kPa (11 psi) to 275.8 kPa (40 psi), 0 kPa (0 psi) to 303.4 kPa (44 psi) and 2 cm to 24 cm respectively. The workspace is calculated using MATLAB `boundary` function with a default `shrink factor` of 0.5.

Dexterity is defined as the ability of the VaLeNS arm end effector to approach a point in its workspace in more than one way or orientation. The different orientations are classified based on the different faces of the "service sphere"[23], [24] shown in Fig. 4(b). Using the results of the workspace analysis, we identify the input actuation parameters (P_b, P_{rc}, P_{rcc}, and L) that lead to the same end effector position but a different end orientation.

C. Experimental Method to Study Stiffness Modulation

Stiffness experiments have been conducted with the VaLeNS arm oriented upside down and applying forces at the end tip of the arm. A linear mechanism is programmed to obtain a displacement of one *cm* by sliding horizontally along its rails for all the scenarios. Reaction forces by the end tip to counter the displacement are recorded using a load cell (FUTEK LRF400 and IPM 650). Two main scenarios were investigated based on similar investigations done in [25].
Scenario 1: The VaLeNS arm is held vertically downwards as shown in Fig. 3(a) and the force is applied laterally to the tip. In this scenario three cases are studied:

1) Case 1: No air pressure in any of the FREEs
2) Case 2: Both rotating actuators actuated to 137.9 kPa (20 psi).
3) Case 3: Both rotating actuators are actuated to 275.8 kPa (40 psi).

Scenario 2: The arm is held vertically and the bending actuator is pressurized to form a 90 degree curved shape, and the force is applied laterally as shown in Fig. 3(e). Three cases are investigated similar to Scenario 1, the only difference is that the bending pressure is adjusted in order to maintain the 90 degree curved shape across all cases for a given length. Each of the above scenarios and cases are conducted across four different extruded lengths of the VaLeNS arm.

D. Deploying the VaLeNS arm on a 3-link robot

The VaLeNS arm is fixed as an additional link on a 3-link rigid robotic base as shown in Fig. 6(a). The rigid robot consists of a rotating base, on which two links (Link 1 and Link2) are assembled. Link 2 is connected to the swiveling servo motor, which in turn is connected to the rigid enclosure housing the SCA. To obtain the forward kinematics of the entire system, the rigid link kinematics is combined with the Kirchhoff model presented earlier. The rigid arm forward kinematics are used to obtain the $\mathbf{p}(s=0)$ and $\mathbf{R}(s=0)$ for the forward model of the soft arm presented in Section III-A. The DYNAMIXEL servos of the 3-link robot are controlled using an Arbotix-M Robocontroller board.

E. Experimental method to study the impact of VaLeNS arm

We study the impact properties of the VaLeNS arm as the maximum force/torque transferred as it contacts an object at varying velocities [26]. First, the VaLeNS arm is mounted on the 3-link robot and its rotating base is operated at different velocities. The end effector of the SCA is made to hit a 3D printed block attached to two 90 degree right hand wound torsional springs (Mcmaster-Carr, 9271K47) in parallel (as shown in Fig. 7(a)-(c)). The 3D printed block attached to the torsional spring is kept at a distance of 50 cm from the base of the 3-link robot arm. The time varying deflection in the spring is measured using a GoPro Hero Session camera at 100 fps. In this paper, the measured maximum deflection of the spring is used to measure the maximum torque exerted by the SCA on the block.

IV. VaLeNS Arm Attributes: Results and Discussions

In this section, we study the different functional attributes of the VaLeNS arm using the analytical and experimental methods detailed in the previous section.

A. Stiffness Modulation

The experimental results reveal that the VaLeNS arm can modulate its stiffness by extruding its length and by simultaneously pressurizing the rotating actuators. Experimental results of all cases of Scenario 1 are shown in Fig. 3(b)-(d). The unpressurized SCA extruded by 4 cm provides a resistive force of 1.1 N when subjected to a 1 cm displacement. The force drastically falls down to 0.08 N when extended to 16 cm. When the SCA rotating actuators are pressurized to 137.9 kPa (20 psi) (case 2) and 275.8 kPa (40 psi) (case 3) respectively, the resistive force for a 4 cm extruded SCA is 1.6N and 1.83 N respectively. Whereas for a 16 cm extruded SCA it is 0.13 N and 0.16 N. Thus there is an increase in stiffness on a scale of approximately 10 times for extruded lengths of 4 cm and 16 cm. There is also a local increase in stiffness by around 49% and 69% when the pressures in the rotating actuators is increased to 137.9 kPa (20 psi) and 275.8 kPa (40 psi) respectively for a 4 cm extruded length. The increase in stiffness for a given length for Scenario 1 is summarized in Table I.

TABLE I

Stiffness results for scenario 1

Scenario 1	Case 1	Case 2	Case 3
Length(cm)	**Stiffness**	**Increase**	**Increase**
4	1.078 N/cm	49%	69%
8	0.3277 N/cm	65%	99%
12	0.1471 N/cm	53%	93%
16	0.0863 N/cm	45%	89%

Similarly, for Scenario 2 the force versus displacement curves are shown in Fig. 3(f)-(h). It can be observed for

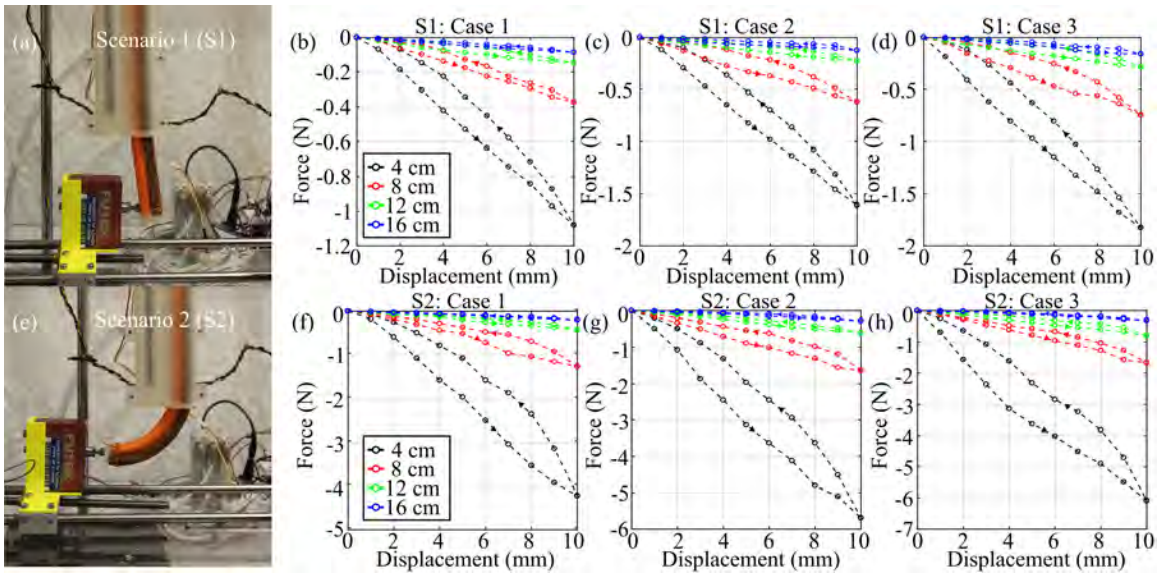

Fig. 3. Stiffness modulation: (a) Experimental setup for scenario 1 and force versus displacement plots for Scenario 1 (b) Case 1 where Rotating (R) actuators pressure is set to 0 kPa, (c) Case 2 where R actuators pressure is set to 137.9 kPa, (d) Case 3 where R actuators pressure is set to 275.8 kPa. (e) Experimental setup for Scenario 2 and force versus displacement plots for Scenario 2 (f) Case 1 (R = 0 kPa), (g) Case 2 (R = 137.9 kPa), (h) Case 3 (R = 275.8 kPa). The arrows indicate the direction of the displacement.

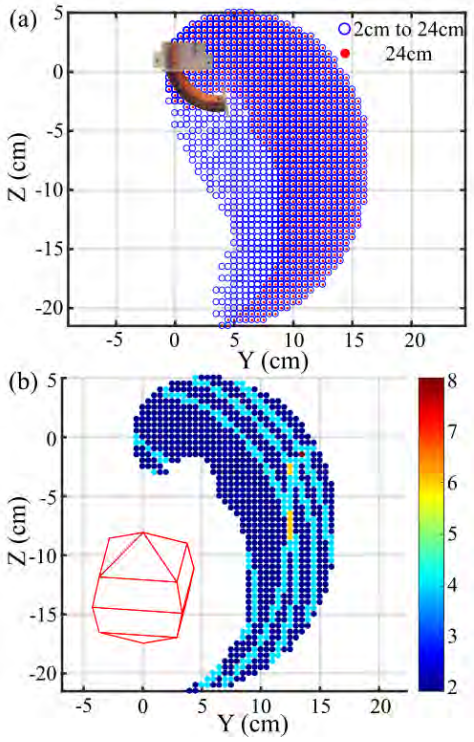

Fig. 4. (a) Workspace of the VaLeNS arm with its entire length extruded (24 cm) and varying extruded lengths (from 2 cm to 24 cm) and (b) Dexterity of the BR^2 SCA with its service sphere shown in the inset. For example, a workspace point with cyan color can be reached in four unique orientations (the center of the service sphere[23] is reached such that the tangents pass through four different faces of the service sphere)

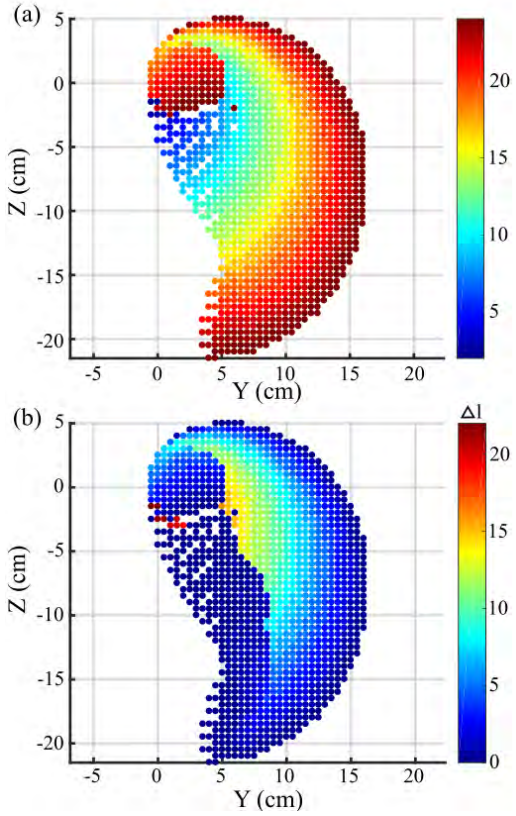

Fig. 5. Reaching a position in different length configurations.(a) Minimum length needed to reach the point lying in YZ plane and (b) The maximum difference in length which can be used to reach a point in the workspace.

case 1 that there is almost a 20 times increase in force for 4 cm when compared with the 16 cm extruded length. An increase in stiffness is also observed in case 2 and case 3. Furthermore, it is observed that there is a 41% and 48% increase in stiffness when the pressure in both the rotating actuators is increased to 137.9 kPa (20 psi) and (275.8 kPa) 40 psi for a 4 cm extruded length. The summarized results for Scenario 2 are shown in Table II. As stated in [27], the stiffness increases in bending configurations.

TABLE II

STIFFNESS RESULTS FOR SCENARIO 2

Scenario 2	Case 1	Case 2	Case 3
Length(cm)	**Stiffness**	**Increase**	**Increase**
4	4.2169 N/cm	35%	44%
8	1.2651 N/cm	30%	32%
12	0.4217 N/cm	45%	88%
16	0.1942 N/cm	41%	57%

B. Workspace and Dexterity

The workspace of the VaLeNS arm can be represented as an axisymmetric surface along the $Y-Z$ plane as shown in Fig. 4(a). Since the arm can rotate about its axis, its actual workspace is a volume of revolution about the arm axis. The workspace of the variable length arm is 1264.5 cm^2 as shown in Fig. 4(a), while the workspace of the fully extended BR^2 (24 cm length) is shown in Fig. 4(b) and is 30% lower than the former.

The dexterity of the VaLeNS arm is due to two features: (a) inherent dexterity of the BR^2 SCA and the (b) variable length mechanism. The inherent dexterity of the BR^2 SCA is due to the combination of several bending and rotation pressures leading to the same end effector position. Figure 4(b) plots the number of different orientations in which each point in the BR^2 workspace can be approached. It can be seen that more than 90% of the workspace can be approached with two or more distinct orientations. To understand the dexterity due to varying length, we evaluate the ability of the arm to reach a position in its workspace with more than one SCA length extruded out. Figure 5(a) plots the minimum SCA length that needs to be extruded to reach a point in the workspace. It is seen that the extreme periphery of the workspace (dark red regions) can be reached with the fully extruded SCA alone. Figure 5(b) plots the difference between the maximum and minimum extruded SCA lengths that can lead to the same end effector position. It is seen that the center area of the workspace can be approached with different extruded lengths. More than 50% of the workspace can be reached with a length difference of 1 cm and around 25% of the workspace can be reached with a length difference of 5 cm. Varying SCA length, as seen in the section above has implications on the stiffness and thus the amount of force

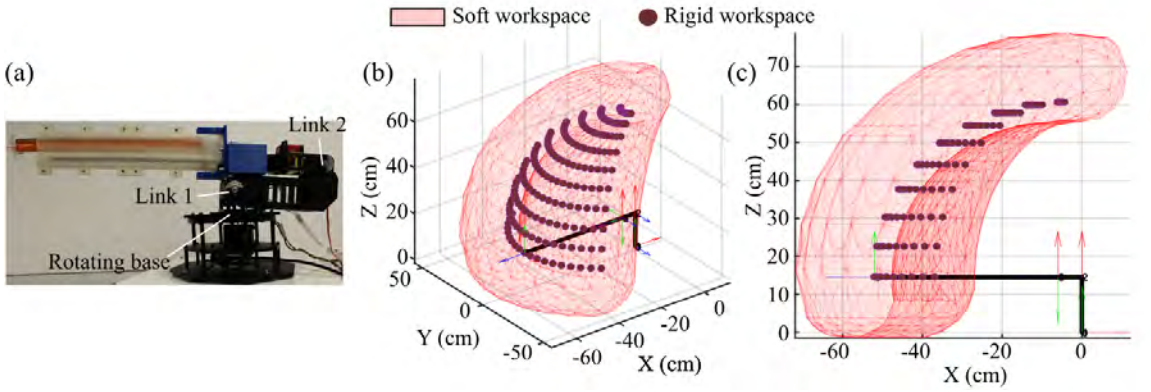

Fig. 6. (a) VaLeNS arm attached to a 3-link robotic arm and its adaptable and precise workspace obtained ((b)isometric view and (c) XZ view) with the ranges of 3 link robotic arm limited to -45 to 45 deg. for the rotating base, Link 1 fixed at 90 deg. and Link 2 varied from 0 deg. to 90 deg.

that can be transmitted during manipulation.

C. Hybrid Workspace

When the VaLeNS arm is deployed on a conventional rigid robot, such as a 3-link rigid arm shown in Fig. 6, its overall workspace will be a combination of the rigid links and the SCA. The implications of the primary attributes studied in the previous subsections (workspace, dexterity and stiffness modulation) can lead to classification of the overall workspace into a rigid workspace and varying levels of soft workspace depending on the extruded arm length as shown in Fig. 6(b)-(c).

In the figure the Link 1 angle is set to 90 degrees and Link 2 is varied from 0 deg. to 90 deg. and the rotating base of the rigid arm is rotated from -45 deg. to 45 deg. and the swiveling base of VaLeNS arm is varied from -90 deg to 90 deg. The rigid workspace is generated from the end positions of the VaLeNS arm when extruded length is 0 cm. It is hypothesized these points can be reached in a quick, accurate and repeatable fashion, a key characteristic of rigid link robots. Furthermore, operating in the rigid workspace will lead to larger force transfer.

The rigid workspace is appended by a larger soft workspace as shown in Fig. 6(b)-(c), which is obtained by extruding the soft arm from 4 cm to 24 cm under the full range of operating pressures. These end positions are hypothesized to be safe as they involve the extruded soft arm and hence can be used for interacting with humans and other fragile objects.

D. Impact test results

The torque obtained by measuring the maximum deflection of torsion spring when the arm contacts the spring with different tangential velocities, and for different extruded lengths is shown in Fig. 7(d). While it is expected for the transmitted torque to decrease with decreased contact velocities, we observe a near 400% decrease in the torque upon extruding the arm by 12 *cm* for all contact velocities. With transmitted impact forces directly correlated to safety especially under human interaction[26], larger extrusion lengths of the VaLeNS arm can be deemed safer.

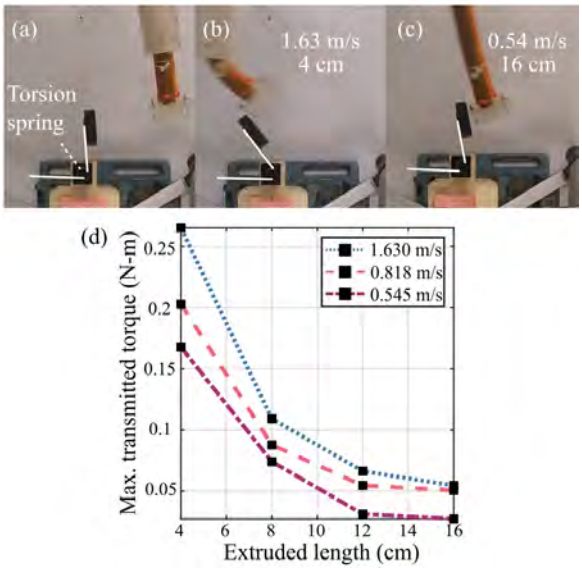

Fig. 7. (a) Impact test setup where a torsion spring is fixed, the maximum deflection of the torsion spring obtained when impacted with the VaLeNS arm extruded to lengths of (b) 4 cm and tangential velcoity 1.63 m/s, (c) 16 cm and tangential velocity 0.54 m/s and (d) maximum transmitted torque when impacted with different SCA extruded lengths and tangential velocities.

V. Demonstration of VaLeNS arm attributes in robotic manipulation tasks

The demonstrations in this section were performed in open loop by manually controlling the 3-link robot arm and the VaLeNS arm in order to accomplish the different tasks. Each of the tasks have been repeated multiple times in order to classify them as a successful/unsuccessful task.

A. Using the VaLeNS arm for a door opening task

To demonstrate the variable stiffness capability of the VaLeNS arm, a door opening task is performed where the door needs to be turned and pulled for the latch to completely open[28]. In Fig. 8(a)-(b) it can be observed that with a 4 cm extruded SCA the arm successfully transfers the force on to the door lock and is able to open it. The SCA is pressurized

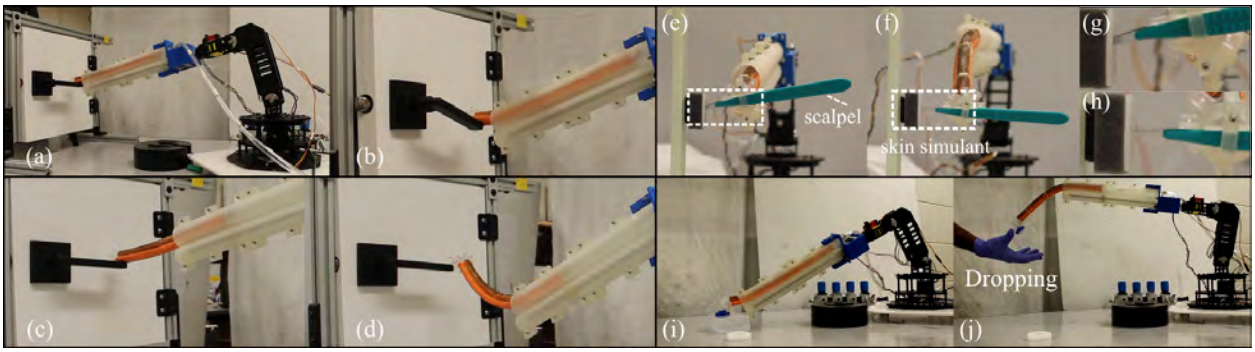

Fig. 8. (a)-(b) Successful door opening with 4 cm extruded SCA, (c)-(d) unsuccessful door opening with 16 cm extruded SCA, (e)-(f) scalpel insertion into a skin simulant when impacted with extruded lengths of 4 cm and 16 cm respectively and (g)-(h) are the enlarged views of (e)-(f) and (i)-(j) picking a box in robots rigid workspace and dropping it in a hand in robots soft workspace

to 275.8 kPa (40 psi) in both the rotating actuators in order to use its high stiffness property(as shown in Fig. 3(d)). Whereas the same task was unsuccessful when the SCA is extruded out by 16 cm as shown in Fig. 8(c)-(d). The door was successfully opened with extruded lengths less than 8 cm with both the rotating actuators of the SCA pressurized to 275.8 kPa (40 psi). Thus, this task required the system to operate closer to its rigid workspace.

B. Using the VaLeNS arm as a Cobot

With its hybrid workspace attribute, the VaLeNS arm attached to a 3 link manipulator can be used as a collaborative robot (Cobot)[29]. We demonstrate an impact test when a skin simulant[30] is stabbed using a scalpel at different extruded lengths and at a velocity of 1.630 m/s in Fig. 8(e) and (f). It was observed that the scalpel could penetrate the skin by 8 mm when the extrusion length of the arm was lowest at 4 cm (Fig. 8(g)). However, at an extrusion length of 16 cm, and keeping the velocity constant at 1.630 m/s, the insertion depth was reduced to 1.3 mm (Fig. 8(h)). Thus the VaLeNS arm with the SCA extruded to larger lengths can be deemed safer as it transfers lower impact energy to the contact object.

The VaLeNS arm can be used in Cobot tasks where both load-bearing ability and safety are required albeit at different time periods. In Fig. 8(i)-(j) it is shown that the robot system with its SCA completely retracted is used to precisely pick up an empty plastic box (Fig. 8(i)). This is accomplished by fitting a suction cup at the end of the SCA. These tasks are performed in the rigid workspace of the arm as sufficient forces are required to be exerted on the objects. The objects are then dropped or handed over to the human safely in the soft workspace as shown in Fig. 8(j) where the SCA is sufficiently extruded.

C. Reachability of the VaLeNS arm

In order to demonstrate the reachability attribute of the VaLeNS arm, an obstacle course is set up as shown in Fig. 9(a)-(b). The arm has to reach two balls located at positions P1 and P2 that are located at a height of 13 cm and 16 cm respectively. These locations are chosen in a way that is not directly accessible from the entry area (in Fig. 9(a)). In order to reach P1 location, the VaLeNS arm is actuated in following sequential fashion (i) SCA extrusion, (ii) SCA bending, (iii) SCA extrusion and (iv) SCA rotation. To reach P2, the VaLeNS arm utilizes a combination of sequential actuation and the aid/support of obstacles [31]. The final reaching poses are shown in Fig. 9(c)-(d). We thus demonstrate that the reachability of the robot is a function of the soft continuum deformation and the variable length deployment.

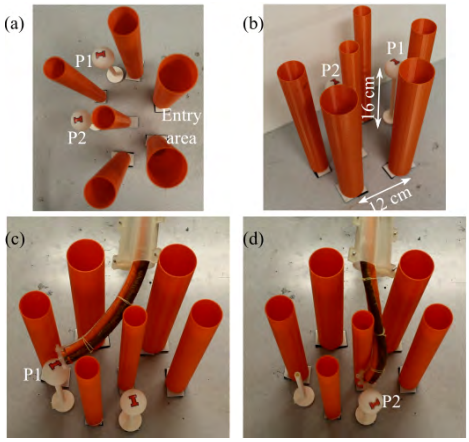

Fig. 9. (a)-(b) Obstacle course for the reachability tests showing the entry area and locations of the objects(P1,P2) to be reached.(c)-(d) final poses of the VaLeNS arm reaching P1 and P2 respectively.

VI. Conclusions

Soft robots and rigid link robots currently represent two extremes in robotic functional space. While soft structures are compliant, safe to interact with and adaptable, rigid link robots are quick, transfer large loads and are precise. However, most emerging robotic applications demand both these functionalities and existing solutions involve a suboptimal compromise. This paper presents a Variable Length Nested Soft (VaLeNS) arm that can toggle between a fully rigid link and varying lengths of a Soft Continuum Arm (SCA). The resulting architecture exhibits two important attributes (i) stiffness modulation, and (ii) enhanced workspace and dexterity. The greatest functional advantage for these

attributes is when the arm is deployed on a rigid robot platform, where its workspace can be bifurcated into a rigid subspace and a soft subspace by just varying the length of the extruded arm. This enables the robotic system to perform precision intensive tasks in the rigid workspace and instantly toggle to the soft workspace to interact safely with humans. Furthermore, combination of arm extrusion and actuation increases reachability, which is useful in navigation in a constrained environment.

The goal of this letter is to introduce the design architecture and the attributes of the VaLeNS arm. However, attesting its real advantages and usefulness calls for a thorough examination and comparison with other modes such as series elastic actuators, and variable stiffness mechanisms in terms of its safety under human interactions, force transfer, and precision. Furthermore, extensive research is required to control such a hybrid system where well-defined rigid robot control meets the less-understood soft arm control space. For an autonomous deployment of the robot, novel soft sensing concepts need to be embedded within the SCA. We propose to explore these areas in the future and objectively evaluate the VaLeNS arm system in applications such as berry harvesting and tasks involving collaborative human robot interactions.

REFERENCES

[1] D. Trivedi, D. Dienno, and C. D. Rahn, "Optimal, Model-Based Design of Soft Robotic Manipulators," *Journal of Mechanical Design*, vol. 130, no. 9, p. 091402, 2008.

[2] D. Rus and M. T. Tolley, "Design, fabrication and control of soft robots," *Nature*, vol. 521, no. 7553, pp. 467–475, 2015.

[3] B. Mazzolai, L. Margheri, M. Cianchetti, P. Dario, and C. Laschi, "Soft-robotic arm inspired by the octopus: II. From artificial requirements to innovative technological solutions," *Bioinspiration & biomimetics*, vol. 7, no. 2, p. 25005, 2012.

[4] C. Laschi, M. Cianchetti, B. Mazzolai, L. Margheri, M. Follador, and P. Dario, "Soft robot arm inspired by the octopus," *Advanced Robotics*, vol. 26, no. 7, pp. 709–727, 2012.

[5] M. Giorelli, F. Renda, M. Calisti, A. Arienti, G. Ferri, and C. Laschi, "Learning the inverse kinetics of an octopus-like manipulator in three-dimensional space," *Bioinspiration & Biomimetics*, vol. 10, no. 3, p. 035006, 5 2015.

[6] W. McMahan, V. Chitrakaran, M. Csencsits, D. Dawson, I. D. Walker, B. A. Jones, M. Pritts, D. Dienno, M. Grissom, and C. D. Rahn, "Field trials and testing of the OctArm continuum manipulator," in *Robotics and Automation, 2006. ICRA 2006. Proceedings 2006 IEEE International Conference on*, 5 2006, pp. 2336–2341.

[7] N. K. Uppalapati, G. Singh, and G. Krishnan, "Parameter estimation and modeling of a pneumatic continuum manipulator with asymmetric building blocks," in *2018 IEEE International Conference on Soft Robotics (RoboSoft)*. IEEE, 4 2018, pp. 528–533.

[8] F. Connolly, C. J. Walsh, and K. Bertoldi, "Automatic design of fiber-reinforced soft actuators for trajectory matching," *Proceedings of the National Academy of Sciences*, vol. 114, no. 1, pp. 51–56, 2017.

[9] J. Li and J. Xiao, "Progressive generation of force-closure grasps for an n-section continuum manipulator," *Proceedings - IEEE International Conference on Robotics and Automation*, no. c, pp. 4016–4022, 2013.

[10] M. Manti, T. G. Thuruthel, F. P. Falotico, A. Pratesi, E. Falotico, M. Cianchetti, and C. Laschi, "Exploiting Morphology of a Soft Manipulator for Assistive Tasks," 2017, pp. 291–301.

[11] P. H. Nguyen, C. Sparks, S. G. Nuthi, N. M. Vale, and P. Polygerinos, "Soft Poly-Limbs: Toward a New Paradigm of Mobile Manipulation for Daily Living Tasks," *Soft Robotics*, vol. 6, no. 1, pp. 38–53, 2 2019.

[12] M. S. Malekzadeh, S. Calinon, D. Bruno, and D. G. Caldwell, "Learning by imitation with the STIFF-FLOP surgical robot: a biomimetic approach inspired by octopus movements," *Robotics and Biomimetics*, vol. 1, no. 1, p. 13, 12 2014.

[13] M. Cianchetti, T. Ranzani, G. Gerboni, I. De Falco, C. Laschi, and A. Menciassi, "STIFF-FLOP surgical manipulator: Mechanical design and experimental characterization of the single module," in *2013 IEEE/RSJ International Conference on Intelligent Robots and Systems*. IEEE, 11 2013, pp. 3576–3581.

[14] D. Trivedi, D. Lesutis, and C. D. Rahn, "Dexterity and Workspace Analysis of Two Soft Robotic Manipulators," in *Volume 2: 34th Annual Mechanisms and Robotics Conference, Parts A and B*, vol. 2010, no. c, American Society of Mechanical Engineers. ASME, 2010, pp. 1389–1398.

[15] I. S. Godage, G. A. Medrano-Cerda, D. T. Branson, E. Guglielmino, and D. G. Caldwell, "Dynamics for variable length multisection continuum arms," *The International Journal of Robotics Research*, vol. 35, no. 6, pp. 695–722, 2016.

[16] P. Dupont, J. Lock, B. Itkowitz, and E. Butler, "Design and Control of Concentric-Tube Robots," *IEEE Transactions on Robotics*, vol. 26, no. 2, pp. 209–225, 4 2010.

[17] E. W. Hawkes, L. H. Blumenschein, J. D. Greer, and A. M. Okamura, "A soft robot that navigates its environment through growth," *Science Robotics*, vol. 2, no. 8, p. eaan3028, 7 2017.

[18] S. Satheeshbabu, N. K. Uppalapati, G. Chowdhary, and G. Krishnan, "Open Loop Position Control of Soft Continuum Arm Using Deep Reinforcement Learning," in *2019 International Conference on Robotics and Automation (ICRA)*. Montreal: IEEE, 5 2019, pp. 5133–5139.

[19] N. K. Uppalapati and G. Krishnan, "Towards Pneumatic Spiral Grippers: Modeling and Design Considerations," *Soft Robotics*, vol. 5, no. 6, pp. 695–709, 12 2018.

[20] C. E. Bryson and D. C. Rucker, "Toward parallel continuum manipulators," *Proceedings - IEEE International Conference on Robotics and Automation*, pp. 778–785, 2014.

[21] D. Trivedi, A. Lotfi, and C. D. Rahn, "Geometrically exact models for soft robotic manipulators," *IEEE Transactions on Robotics*, vol. 24, no. 4, pp. 773–780, 2008.

[22] N. K. Uppalapati and G. Krishnan, "Design of Soft Continuum Manipulators Using Parallel Asymmetric Combination of Fiber Reinforced Elastomers," 8 2018.

[23] L. Wu, R. Crawford, and J. Roberts, "Dexterity Analysis of Three 6-DOF Continuum Robots Combining Concentric Tube Mechanisms and Cable-Driven Mechanisms," *IEEE Robotics and Automation Letters*, vol. 2, no. 2, pp. 514–521, 2017.

[24] M. Badescu and C. Mavroidis, "New performance indices and workspace analysis of reconfigurable hyper-redundant robotic arms," *International Journal of Robotics Research*, vol. 23, no. 6, pp. 643–659, 2004.

[25] A. Shiva, A. Stilli, Y. Noh, A. Faragasso, I. D. Falco, G. Gerboni, M. Cianchetti, A. Menciassi, K. Althoefer, H. A. Wurdemann, I. De Falco, G. Gerboni, M. Cianchetti, A. Menciassi, K. Althoefer, and H. A. Wurdemann, "Tendon-based stiffening for a pneumatically actuated soft manipulator," *IEEE Robotics and Automation Letters*, vol. 1, no. 2, pp. 632–637, 7 2016.

[26] S. Haddadin, A. Albu-Schäffer, and G. Hirzinger, "Requirements for Safe Robots: Measurements, Analysis and New Insights," *The International Journal of Robotics Research*, vol. 28, no. 11-12, pp. 1507–1527, 11 2009.

[27] A. B. Clark and N. Rojas, "Assessing the Performance of Variable Stiffness Continuum Structures of Large Diameter," *IEEE Robotics and Automation Letters*, vol. 4, no. 3, pp. 2455–2462, 2019.

[28] M. Calisti, M. Cianchetti, M. Manti, F. Corucci, and C. Laschi, "Contest-Driven Soft-Robotics Boost: The RoboSoft Grand Challenge," *Frontiers in Robotics and AI*, vol. 3, 9 2016.

[29] S. El Zaatari, M. Marei, W. Li, and Z. Usman, "Cobot programming for collaborative industrial tasks: An overview," *Robotics and Autonomous Systems*, vol. 116, pp. 162–180, 6 2019.

[30] G. Nolan, S. V. Hainsworth, and G. N. Rutty, "Forces generated in stabbing attacks: an evaluation of the utility of the mild, moderate and severe scale," *International Journal of Legal Medicine*, vol. 132, no. 1, pp. 229–236, 1 2018.

[31] J. D. Greer, L. H. Blumenschein, A. M. Okamura, and E. W. Hawkes, "Obstacle-Aided Navigation of a Soft Growing Robot," in *2018 IEEE International Conference on Robotics and Automation (ICRA)*. IEEE, 5 2018, pp. 4165–4172.